Published in IET Electric Power Applications
Received on 27th November 2009
Revised on 22nd March 2010
doi: 10.1049/iet-epa.2009.0281

ISSN 1751-8660

Model for three-phase induction motors with stator core faults

P.M. de la Barrera[1,2] *G.R. Bossio*[1,2] *J.A. Solsona*[1,3] *G.O. García*[1,2]

[1]*Consejo Nacional de Investigaciones Científicas y Técnicas (CONICET), Argentina*
[2]*Grupo de Electrónica Aplicada (GEA), Facultad de Ingeniería, UNRC, Ruta Nacional #36 Km. 601 (X5804BYA), Río Cuarto, Argentina*
[3]*Instituto de Investigaciones en Ingeniería Eléctrica 'Alfredo Desages', Departamento de Ingeniería Eléctrica y de Computadoras, UNS, Av. Alem 1253 (8000), Bahía Blanca, Argentina*
E-mail: pbarrera@ieee.org

Abstract: A new dynamic model for an induction motor (IM) in *abc* machine variables is proposed in this work. This model is able to represent asymmetrical stator core faults (SCF) by modelling them as the variation of the equivalent core loss resistance per phase. One model in *qd0* variables and another one in sequence components are deduced and used as tools to analyse and simulate SCF. It is demonstrated that there is a good correlation between SCF severity and the magnitude of the IM stator negative sequence current, impedance and power. The comparison of simulation and experimental results suggests the validity of the theoretical proposal.

1 Introduction

Stator core faults (SCF) in electrical machines are not as common as those in stator windings. However, costs and repair time of the first ones are much higher [1–3]. For this reason identifying faults causes may be of interest as well as developing strategies to detect them.

Two main causes for SCF are: core melting because of ground fault currents and interlaminar insulation failure [1, 4, 5]. The first one may cause important damage on the core, which would result in an irreversible failure. The second one may be caused by [6]: core abrasion because of the action of strange particles during manufacturing, inspection and/or repair processes; lamination and/or winding vibration; manufacturing defects in lamination and/or in the interlaminar insulation material; and stator–rotor rub during assembly and operation.

There are many off-line methods to detect SCF [7–15]. On-line methods, in general, are widely used because of their low implementation cost since they do not require line production interruption or motor disassembly to detect faults. These methods have been used to detect stator winding turn faults and broken rotor bars [16–21], airgap eccentricity [19, 22] and mechanical load faults [23]. Unfortunately, according to [1], there are no on-line methods available to detect SCF in induction motors (IM) yet.

Based on previous works, the first step in obtaining an on-line fault diagnosis method is the modelling of IM faults. Since SCF produce core loss variations, it is possible to model them as changes in the equivalent core loss resistance (R_{Fe}). This resistance, as proposed in [24], allows representing only core losses symmetrically distributed among the three phases. This model has been widely used in the area of motor control to compensate the detuning effects caused by core losses [24, 25], for example in [26] an on-line core loss resistance estimator was proposed. In addition, a diagnosis strategy for symmetrical SCF based on the previous model was proposed by the authors in [27].

However, in general, the core faults are asymmetrical distributed. Therefore the main objective of this work is obtaining an IM dynamic model in *abc* variables to represent asymmetrical SCF. The model proposed in this

paper is an extension of the model presented in [24]. Here the increase of core losses because of an SCF asymmetrical distributed among the three phases are considered. This increase is taken into account by incorporating three new parameters (ΔR_{Fea}, ΔR_{Feb} and ΔR_{Fec}) in the IM model.

In order to obtain a simulation model, the equations in *qd0* stationary reference frame are deduced from the *abc* model. The equations for the steady-state model in sequence components and in an equivalent circuit are also obtained. The steady-state model allows evaluating the correlation between both the negative sequence stator current and the negative sequence impedance with the SCF severity. Both models can be used as tools to analyse and develop new fault diagnosis strategies.

This work is organised as follows: in Section 2 a new IM model in *abc* variables that includes SCF is proposed; the deduction processes to obtain the *qd0* model is also presented in this section. In Section 3 an IM steady-state model in sequence components are presented. Section 4 displays experimental and simulation results that validate the theoretical proposal. Section 5 draws the main conclusions. In addition, in the Appendix a brief description of the method used by the authors to generate SCF during the experiments is presented.

2 IM dynamic model considering SCF

As it was proposed in [28] iron losses in a magnetic core can be represented by the combination of the equivalent hysteresis resistance and equivalent eddy current resistance that yield an equivalent core loss resistance (R_{Fe}). In the cited paper a detailed physical interpretation of the modelled phenomenon is included.

The same concept proposed in [28] was used in [24–26, 29, 30] to include the core losses in the IM dynamic model with the objective of improving the performance of the machine controller.

From the equivalent circuit proposed in [29], which represents core losses symmetrically distributed among the three phases, a new equivalent circuit, shown in Fig. 1, is proposed in this paper. In this figure, the stator is represented as a stationary circuit (in the figure this is indicated as $\omega = 0$) and the rotor as a rotating circuit (ω_r), both magnetically coupled. The power dissipated in the stator core under normal operation conditions of the IM, for each phase, is represented by the power dissipated in R_{Fe} (rated value of the equivalent core loss resistance). The circuit parameters ΔR_{Fea}, ΔR_{Feb} and ΔR_{Fec} represent the variations of the R_{Fe} in the corresponding phase. These parameters allow representing non-uniformly distributed core losses.

Variations of the per-phase core losses, and therefore ΔR_{Fea}, ΔR_{Feb} and ΔR_{Fec}, between a determined range could be normal in healthy condition of IM. These variations are due to constructional inherent asymmetries such as the rolling direction of the iron sheet [31, 32]. Also, the per-phase core losses can vary during the operation of the machine because of temperature variations [33] or stress (axial and radial) in the core [6, 34]. The variation of core losses outside the range of inherent asymmetries variations would represent an SCF.

An SCF usually generates non-uniformly distributed core losses. Using the model proposed in this paper it is possible to locate SCF into the stator core by adequately valuating ΔR_{Fea}, ΔR_{Feb} and ΔR_{Fec} parameters.

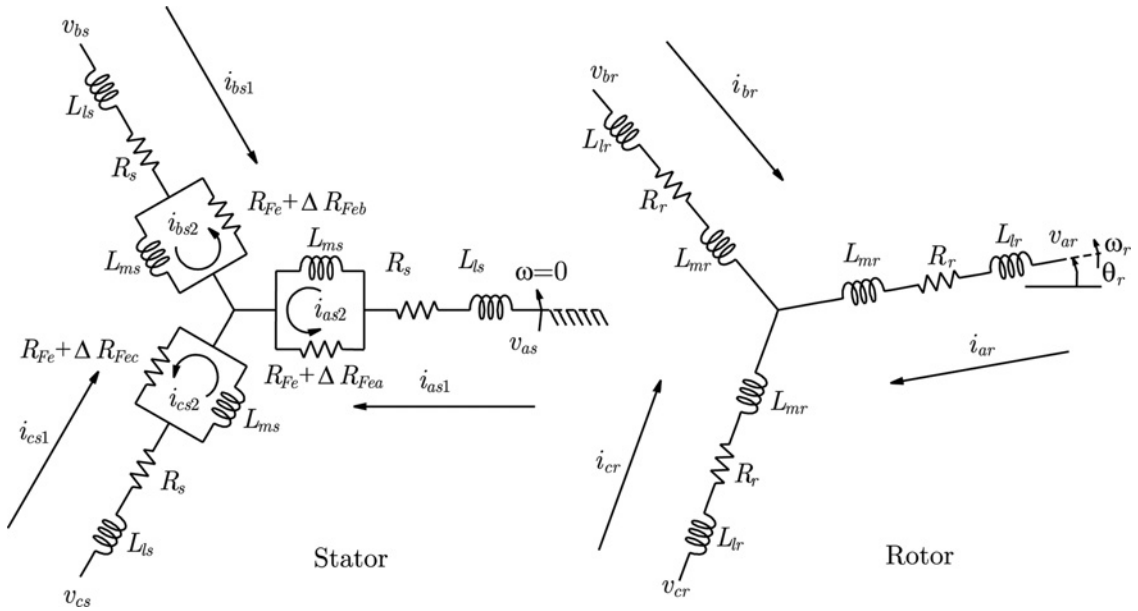

Figure 1 *IM equivalent circuit in abc variables, considering asymmetrical SCF*

IET Electr. Power Appl., 2010, Vol. 4, Iss. 8, pp. 591–602
doi: 10.1049/iet-epa.2009.0281

An SCF means an increase in core losses, therefore the total equivalent core loss resistance for each phase ($R_{\mathrm{Fe}} + \Delta R_{\mathrm{Fe}(\cdot)}$) must decrease. Consequently, $\Delta R_{\mathrm{Fe}a}$, $\Delta R_{\mathrm{Fe}b}$ and $\Delta R_{\mathrm{Fe}c}$ take negative values, with magnitude depending on the fault severity (see [27, 35]) and the location of the fault into the stator core. The relation between core losses and the SCF locations was shown in [36].

2.1 IM equations in abc variables

The stator and rotor voltage equations can be obtained from Fig. 1, as follows

$$\begin{aligned}
\boldsymbol{V}_{abcs} &= \frac{\mathrm{d}}{\mathrm{d}t}\boldsymbol{\psi}_{abcs1} + \boldsymbol{R}_{\mathrm{s}}\boldsymbol{i}_{abcs1} + \boldsymbol{R}_{\mathrm{Fe}}\boldsymbol{i}_{abcs1} - \boldsymbol{R}_{\mathrm{Fe}}\boldsymbol{i}_{abcs2} \\
&\quad + \Delta\boldsymbol{R}_{\mathrm{Fe}}\boldsymbol{i}_{abcs1} - \Delta\boldsymbol{R}_{\mathrm{Fe}}\boldsymbol{i}_{abcs2} \\
\boldsymbol{0} &= \frac{\mathrm{d}}{\mathrm{d}t}\boldsymbol{\psi}_{abcs2} + \boldsymbol{R}_{\mathrm{Fe}}\boldsymbol{i}_{abcs2} - \boldsymbol{R}_{\mathrm{Fe}}\boldsymbol{i}_{abcs1} + \Delta\boldsymbol{R}_{\mathrm{Fe}}\boldsymbol{i}_{abcs2} \\
&\quad - \Delta\boldsymbol{R}_{Fe}\boldsymbol{i}_{abcs1} \\
\boldsymbol{V}_{abcr} &= \frac{\mathrm{d}}{\mathrm{d}t}\boldsymbol{\psi}_{abcr} + \boldsymbol{R}_{\mathrm{r}}\boldsymbol{i}_{abcr}
\end{aligned} \tag{1}$$

where

$$\begin{aligned}
\boldsymbol{V}_{abcs} &= \begin{bmatrix} v_{as} & v_{bs} & v_{cs} \end{bmatrix}^{\mathrm{T}};\ \boldsymbol{V}_{abcr} = \begin{bmatrix} v_{ar} & v_{br} & v_{cr} \end{bmatrix}^{\mathrm{T}} \\
\boldsymbol{i}_{abcs1} &= \begin{bmatrix} i_{as1} & i_{bs1} & i_{cs1} \end{bmatrix}^{\mathrm{T}};\ \boldsymbol{i}_{abcs2} = \begin{bmatrix} i_{as2} & i_{bs2} & i_{cs2} \end{bmatrix}^{\mathrm{T}} \\
\boldsymbol{i}_{abcr} &= \begin{bmatrix} i_{ar} & i_{br} & i_{cr} \end{bmatrix}^{\mathrm{T}} \\
\boldsymbol{\psi}_{abcs1} &= \begin{bmatrix} \psi_{as1} & \psi_{bs1} & \psi_{cs1} \end{bmatrix}^{\mathrm{T}};\ \boldsymbol{\psi}_{abcs2} = \begin{bmatrix} \psi_{as2} & \psi_{bs2} & \psi_{cs2} \end{bmatrix}^{\mathrm{T}} \\
\boldsymbol{\psi}_{abcr} &= \begin{bmatrix} \psi_{ar} & \psi_{br} & \psi_{cr} \end{bmatrix}^{\mathrm{T}} \\
\boldsymbol{R}_{\mathrm{s}} &= R_{\mathrm{s}}\boldsymbol{I}_{3\mathrm{x}3};\ \boldsymbol{R}_{\mathrm{r}} = R_{\mathrm{r}}\,\boldsymbol{I}_{3\mathrm{x}3} \\
\boldsymbol{R}_{\mathrm{Fe}} &= R_{\mathrm{Fe}}\boldsymbol{I}_{3\mathrm{x}3} \\
\Delta\boldsymbol{R}_{\mathrm{Fe}} &= \mathrm{diag}\begin{bmatrix} \Delta R_{\mathrm{Fe}a} & \Delta R_{\mathrm{Fe}b} & \Delta R_{\mathrm{Fe}c} \end{bmatrix}
\end{aligned} \tag{2}$$

Subscripts 1 and 2 represent variables related with stator mesh 1 and 2 in the Fig. 1; subscripts s, r and Fe indicate stator, rotor and iron-related variables, respectively; all rotor variables in (1) are referred to the stator side of the machines; v, i and ψ represent instantaneous voltages, currents and fluxes, respectively, R represents resistances, $\boldsymbol{I}_{3\mathrm{x}3}$ indicates the 3 by 3 identity matrix and superscript T represents the transpose matrix.

The stator and rotor fluxes equations for the IM are

$$\begin{aligned}
\boldsymbol{\psi}_{abcs1} &= \boldsymbol{X}_{\mathrm{ls}}\boldsymbol{i}_{abcs1} \\
\boldsymbol{\psi}_{abcs2} &= \boldsymbol{X}_{\mathrm{ms}}\boldsymbol{i}_{abcs2} + \boldsymbol{X}_{\mathrm{sr}}\boldsymbol{i}_{abcr} \\
\boldsymbol{\psi}_{abcr} &= \boldsymbol{X}_{\mathrm{lr}}\boldsymbol{i}_{abcr} + \boldsymbol{X}_{\mathrm{mr}}\boldsymbol{i}_{abcr} + \boldsymbol{X}_{\mathrm{rs}}\boldsymbol{i}_{abcs2}
\end{aligned} \tag{3}$$

where

$$\boldsymbol{X}_{\mathrm{ls}} = \omega_{\mathrm{b}}L_{\mathrm{ls}}\boldsymbol{I}_{3\mathrm{x}3};\quad \boldsymbol{X}_{\mathrm{lr}} = \omega_{\mathrm{b}}L_{\mathrm{lr}}\boldsymbol{I}_{3\mathrm{x}3}$$

$$\boldsymbol{X}_{\mathrm{ms}} = \boldsymbol{X}_{\mathrm{mr}} = \omega_{\mathrm{b}}L_{\mathrm{m}}\begin{bmatrix} 1 & -\frac{1}{2} & -\frac{1}{2} \\ -\frac{1}{2} & 1 & -\frac{1}{2} \\ -\frac{1}{2} & -\frac{1}{2} & 1 \end{bmatrix}$$

$$\begin{aligned}
\boldsymbol{X}_{\mathrm{sr}} &= \boldsymbol{X}_{\mathrm{rs}}^{\mathrm{T}} \\
&= \omega_{\mathrm{b}}L_{\mathrm{m}}\begin{bmatrix} \cos(\theta_{\mathrm{r}}) & \cos\left(\theta_{\mathrm{r}}+\frac{2\pi}{3}\right) & \cos\left(\theta_{\mathrm{r}}-\frac{2\pi}{3}\right) \\ \cos\left(\theta_{\mathrm{r}}-\frac{2\pi}{3}\right) & \cos(\theta_{\mathrm{r}}) & \cos\left(\theta_{\mathrm{r}}+\frac{2\pi}{3}\right) \\ \cos\left(\theta_{\mathrm{r}}+\frac{2\pi}{3}\right) & \cos\left(\theta_{\mathrm{r}}-\frac{2\pi}{3}\right) & \cos(\theta_{\mathrm{r}}) \end{bmatrix}
\end{aligned}$$

Subscripts l and m indicate leakage and magnetising inductances, respectively, L and $\boldsymbol{X}$ represent inductance and reactance, respectively. θ_{r} and ω_{b} represent the rotor position and the base electrical angular frequency, respectively.

The electromagnetic torque can be calculated in *abc* variables as in [37]

$$T_{\mathrm{e}} = \left(\frac{1}{\omega_{\mathrm{b}}}\right)\left(\frac{P}{2}\right)(\boldsymbol{i}_{abcs2})^{\mathrm{T}}\frac{\partial}{\partial\theta_{\mathrm{r}}}[\boldsymbol{X}_{\mathrm{sr}}]\boldsymbol{i}_{abcr} \tag{4}$$

where P is the number of poles of the IM and $\partial/\partial\theta_{\mathrm{r}}$ represents the partial derivative with respect to the rotor position.

2.2 IM equations in qd0 variables

In order to obtain a simulation model, the equations in *qd0* stationary reference frame will be deduced from the *abc* model.

By transforming (1) and (3) to the stationary reference frame [37], the IM equations in *qd0* variables can be expressed as

$$\begin{aligned}
\boldsymbol{V}_{qd0\mathrm{s}} &= \frac{1}{\omega_{\mathrm{b}}}\frac{\mathrm{d}}{\mathrm{d}t}\boldsymbol{\psi}_{qd0\mathrm{s}1} + \boldsymbol{R}_{\mathrm{s}}\boldsymbol{i}_{qd0\mathrm{s}1} + \boldsymbol{R}_{\mathrm{Fe}}(\boldsymbol{i}_{qd0\mathrm{s}1} - \boldsymbol{i}_{qd0\mathrm{s}2}) \\
&\quad + \Delta\boldsymbol{R}_{\mathrm{Fe}qd0}(\boldsymbol{i}_{qd0\mathrm{s}1} - \boldsymbol{i}_{qd0\mathrm{s}2})
\end{aligned} \tag{5}$$

$$\boldsymbol{0} = \frac{1}{\omega_b}\frac{\mathrm{d}}{\mathrm{d}t}\boldsymbol{\psi}_{qd0\mathrm{s}2} + \boldsymbol{R}_{\mathrm{Fe}}(\boldsymbol{i}_{qd0\mathrm{s}2} - \boldsymbol{i}_{qd0\mathrm{s}1}) + \Delta\boldsymbol{R}_{\mathrm{Fe}qd0}(\boldsymbol{i}_{qd0\mathrm{s}2} - \boldsymbol{i}_{qd0\mathrm{s}1}) \tag{6}$$

$$\boldsymbol{V}_{qd0\mathrm{r}} = \left(\frac{\omega_{\mathrm{r}}}{\omega_{\mathrm{b}}}\right)\boldsymbol{J}\boldsymbol{\psi}_{qd0\mathrm{r}} + \frac{1}{\omega_{\mathrm{b}}}\frac{\mathrm{d}}{\mathrm{d}t}\boldsymbol{\psi}_{qd0\mathrm{r}} + \boldsymbol{R}_{\mathrm{r}}\boldsymbol{i}_{abcr} \tag{7}$$

where

$$\boldsymbol{J} = \begin{bmatrix} 0 & -1 & 0 \\ 1 & 0 & 0 \\ 0 & 0 & 0 \end{bmatrix}$$

The flux equations are

$$\begin{aligned} \boldsymbol{\psi}_{qd0\mathrm{s}1} &= \boldsymbol{X}_{\mathrm{ls}qd0}\boldsymbol{i}_{qd0\mathrm{s}1} \\ \boldsymbol{\psi}_{qd0\mathrm{s}2} &= \boldsymbol{X}_{\mathrm{ms}qd0}\boldsymbol{i}_{qd0\mathrm{s}2} + \boldsymbol{X}_{\mathrm{sr}qd0}\boldsymbol{i}_{qd0\mathrm{r}} \\ \boldsymbol{\psi}_{qd0\mathrm{r}} &= \boldsymbol{X}_{\mathrm{lr}qd0}\boldsymbol{i}_{qd0\mathrm{r}} + \boldsymbol{X}_{\mathrm{mr}qd0}\boldsymbol{i}_{qd0\mathrm{r}} + \boldsymbol{X}_{\mathrm{rs}qd0}\boldsymbol{i}_{qd0\mathrm{s}2} \end{aligned} \tag{8}$$

where

$$\boldsymbol{X}_{\mathrm{ls}qd0} = \omega_{\mathrm{b}} L_{\mathrm{ls}} \boldsymbol{I}_{3\mathrm{x}3}$$

$$\boldsymbol{X}_{\mathrm{lr}qd0} = \omega_{\mathrm{b}} L_{\mathrm{lr}} \boldsymbol{I}_{3\mathrm{x}3}$$

$$\boldsymbol{X}_{\mathrm{ms}qd0} = \omega_{\mathrm{b}} M \mathrm{diag}\begin{bmatrix} 1 & 1 & 0 \end{bmatrix}$$

$$\boldsymbol{X}_{\mathrm{mr}qd0} = \omega_{\mathrm{b}} M \mathrm{diag}\begin{bmatrix} 1 & 1 & 0 \end{bmatrix}$$

$$M = \frac{3}{2} L_{\mathrm{m}}; \quad \omega_{\mathrm{r}} = \frac{\mathrm{d}}{\mathrm{d}t}\theta_{\mathrm{r}}$$

$$\boldsymbol{X}_{\mathrm{sr}qd0} = \omega_{\mathrm{b}} M \mathrm{diag}\begin{bmatrix} 1 & 1 & 0 \end{bmatrix}$$

The matrix that represents core loss variations in *qd0* variables is given by (see (9))

The electromagnetic torque in *qd0* variables can be calculated by substituting the transformed variables into (4), yielding

$$T_{\mathrm{e}} = \left(\frac{3}{2}\right)\left(\frac{P}{2}\right)\left(\frac{X_{\mathrm{m}}}{\omega_{\mathrm{b}}}\right)(i_{qs2} i_{d\mathrm{r}} - i_{ds2} i_{q\mathrm{r}}) \tag{10}$$

where i_{qs2} and i_{ds2} are the quadrature and direct components of $\boldsymbol{i}_{qd0\mathrm{s}2}$, respectively; $i_{q\mathrm{r}}$ and $i_{d\mathrm{r}}$ are the quadrature and direct components of $\boldsymbol{i}_{qd0\mathrm{r}}$, respectively.

The simulation model used in Section 4 to analyse the effects of the IM SCF was obtained by reorganising the previous equations.

Some comments are submitted below to facilitate the understanding of the physical interpretation of the proposed model.

- When core losses are non-uniformly distributed ($\Delta R_{\mathrm{Fe}a}$, $\Delta R_{\mathrm{Fe}b}$ and $\Delta R_{\mathrm{Fe}c}$ are not equal), (9) is a non-symmetrical full matrix and generates the fourth term in (5).

- When core losses are uniformly distributed, (9) is a diagonal matrix with equal entries in its diagonal and the fourth term of (5) can be combined with the third one yielding the same model presented in [29].

- If core losses phenomenon are not considered ($R_{\mathrm{Fe}} \to \infty$), the third and fourth terms are zero yielding the conventional dynamic IM model [37].

From the previous considerations, it can be remarked that the conventional dynamic IM model [37] and the model proposed in [29] are particular cases of the model proposed in this paper.

3 IM steady-state model sequence components

The main objective of this section is to analyse the effect of SCF on the variables of the IM in steady state at rated frequency. For this reason, a new steady-state model in sequence components is presented in this section. This model can be obtained from the IM dynamic model in *abc* variables presented in Section 2 and by applying the symmetrical-components method. It consists in representing a set of variables called sequence components ($\boldsymbol{f}_{+-0}$) in terms of the three-phase variables ($\boldsymbol{f}_{abc}$) [38], as follows

$$\boldsymbol{f}_{+-0} = \boldsymbol{S}^{-1}\boldsymbol{f}_{abc} \tag{11}$$

where

$$\begin{aligned} \boldsymbol{f}_{abc} &= \begin{bmatrix} f_a & f_b & f_c \end{bmatrix}^{\mathrm{T}} \\ \boldsymbol{f}_{+-0} &= \begin{bmatrix} f_+ & f_- & f_0 \end{bmatrix}^{\mathrm{T}} \\ \boldsymbol{S} &= \begin{bmatrix} 1 & 1 & 1 \\ a^2 & a & 1 \\ a & a^2 & 1 \end{bmatrix}; \boldsymbol{S}^{-1} = \frac{1}{3}\begin{bmatrix} 1 & a & a^2 \\ 1 & a^2 & a \\ 1 & 1 & 1 \end{bmatrix} \\ a &= \mathrm{e}^{\mathrm{j}\frac{2}{3}\pi} \end{aligned} \tag{12}$$

where f is a generic instantaneous variable that represents voltages, currents or fluxes. The subscripts $+$, $-$ and 0 represent the positive, negative and zero sequence components, respectively.

$$\boldsymbol{\Delta R}_{\mathrm{Fe}qd0} = \frac{2}{3}\begin{bmatrix} \Delta R_{\mathrm{Fe}a} + \frac{1}{4}\Delta R_{\mathrm{Fe}b} + \frac{1}{4}\Delta R_{\mathrm{Fe}c} & \left(\frac{\sqrt{3}}{4}\right)(\Delta R_{\mathrm{Fe}b} - \Delta R_{\mathrm{Fe}c}) & \left(\Delta R_{\mathrm{Fe}a} - \frac{1}{2}\Delta R_{\mathrm{Fe}b} - \frac{1}{2}\Delta R_{\mathrm{Fe}c}\right) \\ \left(\frac{\sqrt{3}}{4}\right)(\Delta R_{\mathrm{Fe}b} - \Delta R_{\mathrm{Fe}c}) & \left(\frac{3}{4}\right)(\Delta R_{\mathrm{Fe}b} + \Delta R_{\mathrm{Fe}c}) & -\left(\frac{\sqrt{3}}{2}\right)(\Delta R_{\mathrm{Fe}b} - \Delta R_{\mathrm{Fe}c}) \\ \left(\frac{1}{2}\Delta R_{\mathrm{Fe}a} - \frac{1}{4}\Delta R_{\mathrm{Fe}b} - \frac{1}{4}\Delta R_{\mathrm{Fe}c}\right) & -\left(\frac{\sqrt{3}}{4}\right)(\Delta R_{\mathrm{Fe}b} - \Delta R_{\mathrm{Fe}c}) & \left(\frac{1}{2}\right)(\Delta R_{\mathrm{Fe}a} + \Delta R_{\mathrm{Fe}b} + \Delta R_{\mathrm{Fe}c}) \end{bmatrix} \tag{9}$$

IET Electr. Power Appl., 2010, Vol. 4, Iss. 8, pp. 591–602
doi: 10.1049/iet-epa.2009.0281

If the transformation (12) is applied to (1) and (3), and the IM is considered as working at sinusoidal steady state (see [38]), the following equations can be obtained

$$\begin{aligned}\tilde{V}_{+s} &= \tilde{Z}_s\tilde{I}_{+s1} + (R_{Fe} + \Delta R_{Fe})(\tilde{I}_{+s1} - \tilde{I}_{+s2} + \tilde{I}_{+f})\\ \tilde{V}_{-s} &= \tilde{Z}_s\tilde{I}_{-s1} + (R_{Fe} + \Delta R_{Fe})(\tilde{I}_{-s1} - \tilde{I}_{-s2} + \tilde{I}_{-f})\\ \tilde{V}_{0s} &= \tilde{Z}_s\tilde{I}_{0s1} + (R_{Fe} + \Delta R_{Fe})(\tilde{I}_{0s1} - \tilde{I}_{0s2} + \tilde{I}_{0f})\end{aligned} \quad (13)$$

$$\begin{aligned}0 &= j\omega_e M(\tilde{I}_{+s2} + \tilde{I}_{+r}) + (R_{Fe} + \Delta R_{Fe})(\tilde{I}_{+s2} - \tilde{I}_{+s1} - \tilde{I}_{+f})\\ 0 &= j\omega_e M(\tilde{I}_{-s2} + \tilde{I}_{-r}) + (R_{Fe} + \Delta R_{Fe})(\tilde{I}_{-s2} - \tilde{I}_{-s1} - \tilde{I}_{-f})\\ 0 &= (R_{Fe} + \Delta R_{Fe})(\tilde{I}_{0s2} - \tilde{I}_{0s1} - \tilde{I}_{0f})\end{aligned} \quad (14)$$

$$\begin{aligned}0 &= \left(\frac{R_r}{s} + j\omega_e L_{lr}\right)\tilde{I}_{+r} + j\omega_e M(\tilde{I}_{+s2} + \tilde{I}_{+r})\\ 0 &= \left(\frac{R_r}{2-s} + j\omega_e L_{lr}\right)\tilde{I}_{-r} + j\omega_e M(\tilde{I}_{-s2} + \tilde{I}_{-r})\end{aligned} \quad (15)$$

where

$$\begin{aligned}\tilde{Z}_s &= R_s + j\omega_e L_{ls}\\ \frac{1}{s} &= \frac{\omega_e}{\omega_e - \omega_r};\ \frac{1}{2-s} = \frac{\omega_e}{\omega_e + \omega_r}\\ \Delta R_{Fe} &= \frac{1}{3}(\Delta R_{Fea} + \Delta R_{Feb} + \Delta R_{Fec})\end{aligned} \quad (16)$$

ω_e and ω_r represent the electrical angular frequency and the rotor angular speed, respectively. $\tilde{V}$ and $\tilde{I}$ represent the phasors of the voltage and current, respectively, and can be represented as

$$\tilde{V} = \bar{V}\sqrt{2}e^{j\alpha_V};\ \tilde{I} = \bar{I}\sqrt{2}e^{j\alpha_I}$$

$\bar{V}$ and $\bar{I}$ represent RMS values of the sinusoidal voltage and current, respectively; α is the phase of the phasor.

SCF currents $\tilde{I}_{+f}$, $\tilde{I}_{-f}$ and $\tilde{I}_{0f}$ are given by (see (17))

It can be seen in (17) that the SCF currents are a consequence of the equivalent core loss resistance variation per phase or the asymmetries due to SCF. The existence of an SCF produces a coupling between the different sequence currents that can be appreciated in (17), which in turns affects (13).

The equivalent circuit shown in Fig. 2 represents the IM model in sequence components. It can be obtained by inspection from (13) to (15). The SCF currents are represented by three current sources in this circuit. SCF can be analysed and evaluated in this circuit through analysing the current injected by the current sources and by the variation of ΔR_{Fe} (16).

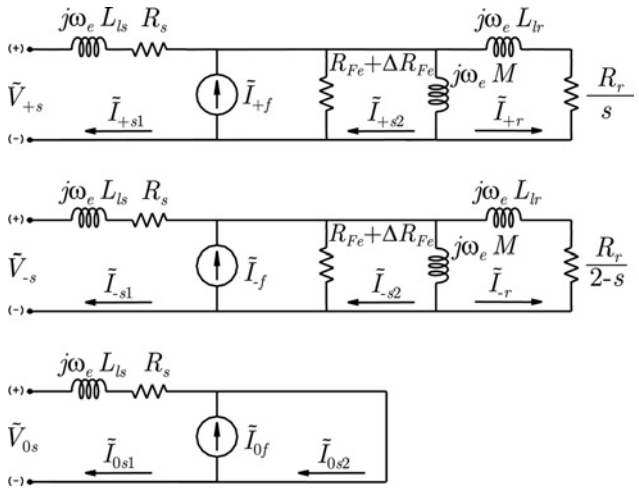

Figure 2 *IM equivalent circuits in sequence components considering asymmetrical SCF*

It is interesting to observe in Fig. 2 that even when $\tilde{V}_{-s}$ is zero (balanced supply voltage), $\tilde{I}_{-s1}$ is not zero under SCF conditions. That is due to the coupling phenomenon mentioned above. Then, it can be concluded that $\tilde{I}_{-s1}$ can represent the SCF severity.

From a practical point of view, it is possible to measure $\tilde{I}_{-s1}$ with the objective of estimating the SCF severity when $\tilde{V}_{-s}$ is zero. Another way to estimate the SCF severity is to calculate the impedance from $\tilde{V}_{-s}$ and $\tilde{I}_{-s1}$, when voltage is unbalanced. It is worth mentioning that, the sensitivity of this impedance with respect to unbalance supply voltage amplitude is not important.

It is well known that similar effects than those generated by SCF are produced by winding turn faults and high-resistance electrical connection [39, 40]. In the opinion of the authors, one possibility in an attempt to discriminate the effects of each fault is extending the analysis of the impedance matrix done in [41] and/or the analysis of $\tilde{I}_{-s1}$ done in [39].

$$\begin{aligned}\tilde{I}_{+f} &= \frac{(\Delta R_{Fea} + a^2\Delta R_{Feb} + a\Delta R_{Fec})(\tilde{I}_{-s1} - \tilde{I}_{-s2}) + (\Delta R_{Fea} + a\Delta R_{Feb} + a^2\Delta R_{Fec})(\tilde{I}_{0s1} - \tilde{I}_{0s2})}{3(R_{Fe} + \Delta R_{Fe})}\\ \tilde{I}_{-f} &= \frac{(\Delta R_{Fea} + a\Delta R_{Feb} + a^2\Delta R_{Fec})(\tilde{I}_{+s1} - \tilde{I}_{+s2}) + (\Delta R_{Fea} + a^2\Delta R_{Feb} + a\Delta R_{Fec})(\tilde{I}_{0s1} - \tilde{I}_{0s2})}{3(R_{Fe} + \Delta R_{Fe})}\\ \tilde{I}_{0f} &= \frac{(\Delta R_{Fea} + a^2\Delta R_{Feb} + a\Delta R_{Fec})(\tilde{I}_{+s1} - \tilde{I}_{+s2}) + (\Delta R_{Fea} + a\Delta R_{Feb} + a^2\Delta R_{Fec})(\tilde{I}_{-s1} - \tilde{I}_{-s2})}{3(R_{Fe} + \Delta R_{Fe})}\end{aligned} \quad (17)$$

4 Experimental validation

The experimental set-up is briefly introduced in the following section. In the last section, simulation and experimental results are compared and discussed in detail with the objective of validating the proposed models.

4.1 Experimental set-up

Fig. 3 shows the complete laboratory set-up used in this paper to obtain the experimental results. This set-up consists of a standard 5.5 kW squirrel cage IM supplied by the network ('Under test' in the figure). The rated variables of the IM are shown in Table 1. This IM is coupled to another IM supplied by a commercial torque-controlled variable speed drive, which acts as a programmable load.

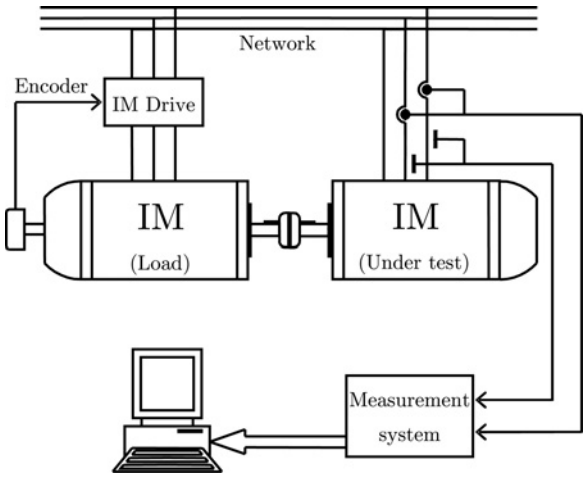

Figure 3 *Experimental set-up*

Table 1 IM technical data and parameters

Variable	Value	Parameter	Value
P_n (kW/HP)	5.5/7.5	R_s (Ω)	0.9267
V_n (V)	220/380	R_r (Ω)	2.06
I_n (A)	19.9/11.1	R_{Fe} (Ω)	156.997
f (Hz)	50	$L_{ls} = L_{lr}$ (mH)	4.67
T_n (Nm)	35.00	M (mH)	155.597
cosϕ	0.82		

Two phase currents and two line voltages were logged and measured by an oscillographic recorder ('measurement system') with a sampling frequency of 8 kHz and 12 bit of resolution. Finally, these electric signals were processed by a PC.

As part of the experiments, SCF were produced in the IM under test using the method proposed in [35] and summarised in the Appendix.

4.2 Experimental and simulation results

The experimental results presented in this section were obtained with three different asymmetrical SCF severities that were performed, as it was pointed out in the previous section, with the method proposed in [35]. The first column of Table 2 shows the percentage of faulted lamination (short-circuited), in one slot of the stator core, with respect to the total lamination (0% represents the healthy motor).

For the different fault conditions, instantaneous power was calculated from the measuring signals of input voltages and currents and then the total no-load power (P_0) was calculated by integration. In addition, the core losses (P_{Fe}) were estimated based on P_0, stator copper losses (I^2R_s) and windage and friction losses. The latter losses were determined as it was proposed in [42], through a set of no-load tests at different supply voltages. Because the IM is working at no-load the rotor copper losses were neglected.

Second and third columns of Table 2 show P_0 and P_{Fe} for the different fault conditions. A significant increase of both quantities because of SCF can be clearly observed; this fact is consistent with the results obtained in [35].

Based on P_0 for the different SCF severities, the new parameters (ΔR_{Fea}, ΔR_{Feb} and ΔR_{Fec}) of the proposed IM model were adjusted. The other parameters of the IM were determined by performing the no-load and locked-rotor tests [37] and they are listed in Table 2.

With the objective of adjusting the new parameters of the IM, real faults were performed. They were located 90 electrical degree apart from the magnetic axis of the phase a, as can see in Fig. 4. In this position, the increase of the P_{Fe} because of the SCF for that phase is in its maximum value because the flux in the yoke is maximum [36]. As it can be seen in Fig. 4,

Table 2 Experimental data for stator core faults

% of faulted laminations	P_0, W	P_{Fe}, W	ΔR_{Fea}, Ω	η, %	$\eta_{P_{Fe}}$, %
0	976.43	870.88	0	0	0
30	986.70	880.10	−11.20	1.051	1.058
65	1055.04	947.21	−34.02	8.050	8.764
100	1081.80	972.19	−40.01	10.791	11.633

doi: 10.1049/iet-epa.2009.0281

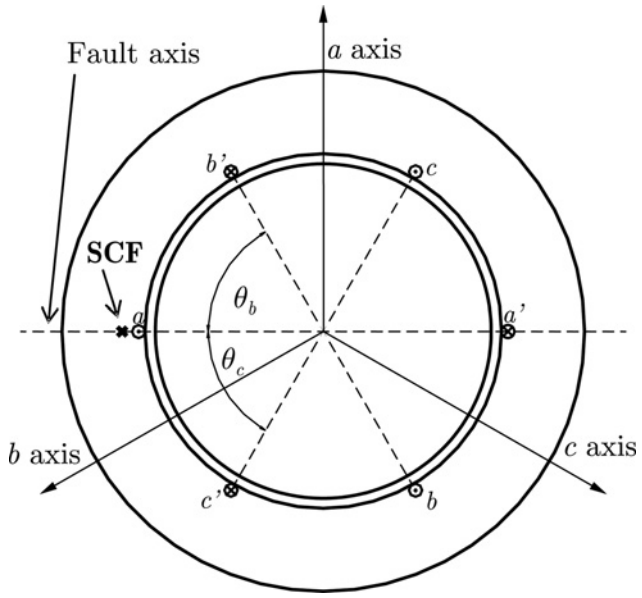

Figure 4 *Location of the SCF in the IM*

the angle between the fault axis and the other phases (*b* and *c*) is the same. In this way, the increase of the power in each phase is also the same and much smaller than that of phase *a*.

The theoretical fact pointed out in the last paragraph is shown in Fig. 5, it depicts the increase of P_{Fe} per phase for different fault severities in p.u. of P_{Fe} per phase for no-fault conditions. The figure shows an important increase of the losses in phase *a* (fault location) whereas in the other phases (*b* and *c*) the losses remain almost constant and they are an order smaller than the first one.

Therefore and just to simplify, the SCF were modelled and simulated as concentrated in the phase *a*, considering that the influence on the other phases are negligible. Hence, the parameters $\Delta R_{\mathrm{Fe}b}$ and $\Delta R_{\mathrm{Fe}c}$ were considered zero and $\Delta R_{\mathrm{Fe}a}$ was adjusted so as to produce the same no-load power (P_0) than that produced by a real SCF, see Table 2.

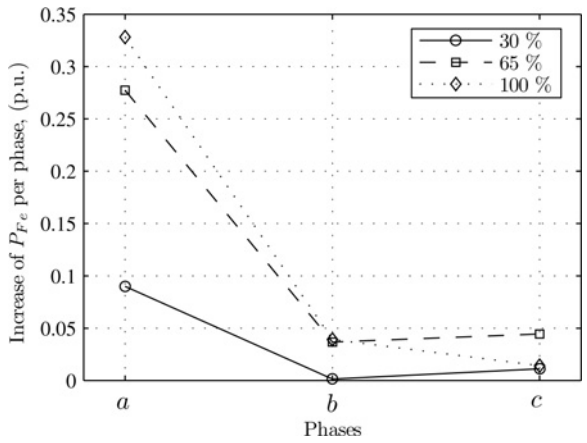

Figure 5 *Increase of P_{Fe} per phase for different percentage of faulted lamination*

Table 2 also displays, in its fifth column, the SCF severity factor (η) for different fault severity conditions. This factor was defined as the increase of P_0 for each fault condition with respect to the no-fault condition, expressed in percent (%) of P_0 for no-fault conditions, as

$$\eta = \frac{P_{0_{(\mathrm{faulted})}} - P_{0_{(\mathrm{no-faulted})}}}{P_{0_{(\mathrm{no-faulted})}}} 100\% \tag{18}$$

The last column of Table 2 shows the SCF severity factor calculated with the core losses ($\eta_{P_{\mathrm{Fe}}}$), in the same way as for η. This value ($\eta_{P_{\mathrm{Fe}}}$) quantify the influence of SCF more precisely than η, but in a practical point of view η is easier to determine. In addition, the error between both severity factors is small, as can be seen from the table. Therefore in this paper η will be used.

The range of severity evaluated and shown in this section can be considered as incipient SCF since the most severe case just produces an increase in P_{Fe} of 11.63%.

Fig. 6 shows simulation results for the SCF currents against the SCF severity factor. It is observed in the same figure that the increase in $\tilde{I}_{-f}$ against the SCF severity factor is much higher than that of the other two currents. It can be concluded from these results that $\tilde{I}_{-f}$ shows the highest sensitivity to estimate the SCF severity. From a practical point of view the variation of $\tilde{I}_{-f}$ can be detected through measuring $\tilde{I}_{-\mathrm{s1}}$ when $\tilde{V}_{-\mathrm{s}}$ is zero (balanced voltage supply).

A real IM has inherent asymmetries and then $\tilde{I}_{-\mathrm{s1}}$ is not zero. Therefore it was necessary to compensate that fact to properly compare simulation and experimental results. For this objective to be achieved, the negative-sequence stator current increment ($\Delta\tilde{I}_{-\mathrm{s1}}$), in p.u. of the IM rated current (I_n), was defined. This increment was calculated as the difference between the negative sequence stator currents under SCF conditions and those for no-fault conditions.

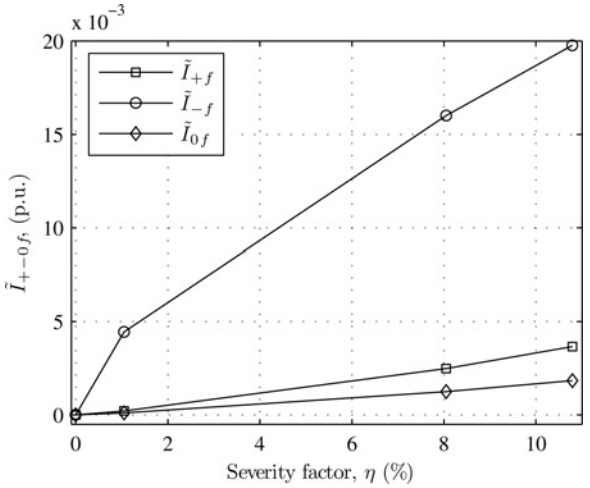

Figure 6 *Simulation results for the SCF currents*

Figs. 7*a* and *b* show experimental (solid line) and simulation (dashed line) results for the negative-sequence stator current increment ($\Delta\tilde{I}_{-s1}$) against the SCF severity factor for no-load and for 40% load, respectively. These results were obtained under balanced supply voltage conditions. From these figures, it can be concluded that simulation and experimental data show a similar behaviour and $\Delta\tilde{I}_{-s1}$ remains almost unchanged for load torque variations. Based on their experience, the authors think that the differences between simulation and experimental results can be explained because of the uncertainty in the IM parameters and inherent asymmetries that are highly load dependent. These inherent asymmetries can be expressed in additive or subtractive form depending on the conditions, as can be seen in Fig. 7*b*.

As it was suggested in Section 3, another possibility to estimate the SCF severity is to analyse the behaviour of the IM input negative sequence impedance magnitude ($|\boldsymbol{Z}_-|$). This value is calculated from the IM sequence component impedance matrix. However, it cannot be determined with only one measured set of voltages and currents because off-diagonal terms of the impedance matrix appear. Although $|\boldsymbol{Z}_-|$ can be approximated by (19), according to [43]

$$|\boldsymbol{Z}_-| = \frac{|\tilde{V}_{-s}|}{|\tilde{I}_{-s1}|} \tag{19}$$

where $|\cdot|$ indicates modulus (magnitude).

Fig. 8*a* shows simulation (dashed line) and experimental results (solid line) for $|\boldsymbol{Z}_-|$ against the SCF severity factor. These results were obtained from applying an unbalanced supply voltage of about 3%, ($[|\tilde{V}_{-s}|/|\tilde{V}_{+s}|]100$) = 3% and a load level of 75%. The load level of 75% was chosen because $|\boldsymbol{Z}_-|$ is highly influenced by light load level in motors with closed rotor slots, as it was demonstrated in [31] and [44]. These results show that a decrease of $|\boldsymbol{Z}_-|$

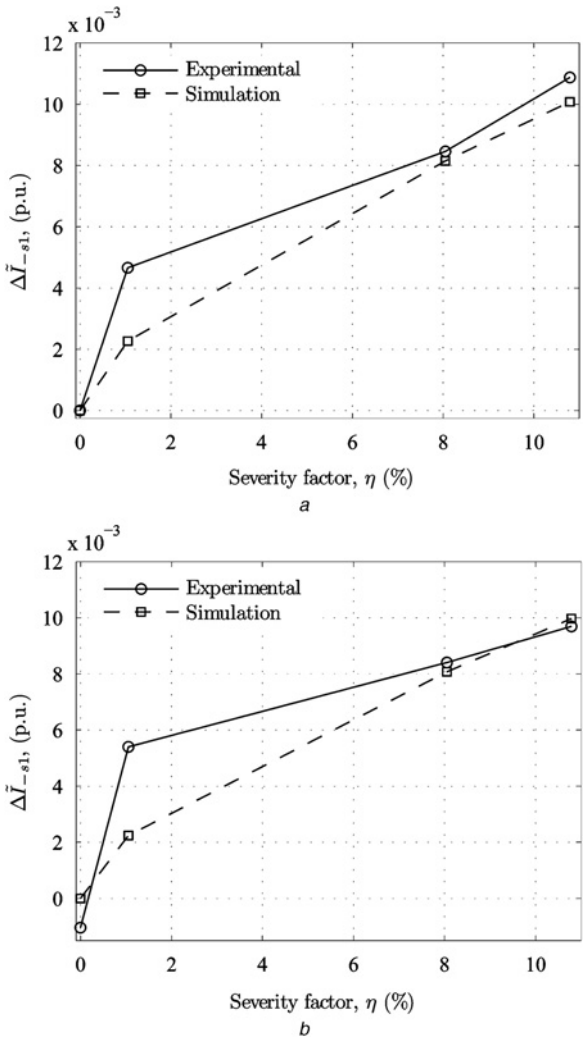

Figure 7 *Experimental and simulation results for* $\Delta\tilde{I}_{-s1}$

a At no-load
b At 40% load

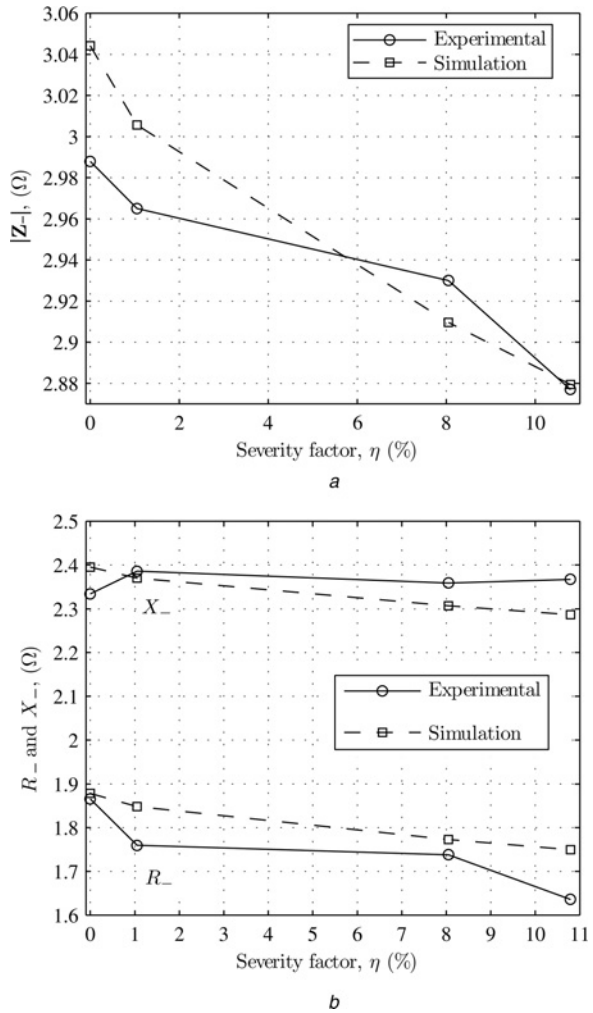

Figure 8 *Experimental and simulation results for the negative-sequence impedance at 75% load and 3% of unbalanced supply voltage*

a Modulus (magnitude)
b Real and imaginary parts of $\boldsymbol{Z}_-$

IET Electr. Power Appl., 2010, Vol. 4, Iss. 8, pp. 591–602
doi: 10.1049/iet-epa.2009.0281

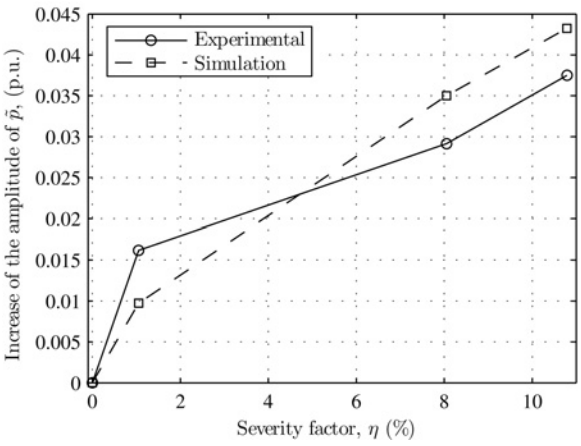

Figure 9 *Experimental and simulation results for the amplitude increase of $2\omega_e$ component of p at no-load and balanced supply voltage*

corresponds to an increase of η. A difference between simulation and experimental results can be observed when the SCF severity factor is low. This difference occurs because IM inherent asymmetries and the uncertainty in parameters produce effects of the same order than those produced by fault when the SCF severity factor is low.

Simulation and experimental results for both, real ($R\_$) and imaginary ($X\_$) parts of the input negative sequence impedance can be observed in Fig. 8*b*. The same figure shows that as the severity factor increases, $R\_$ decreases faster than $X\_$, because of the variation of ΔR_{Fea}.

The increase of the negative sequence current also produces an increase in the oscillating component of the active power (p) at a frequency of $2\omega_e$. Fig. 9 shows the amplitude increase of $2\omega_e$ component of p, in p.u. of IM rated total power, against SCF severity factor. As it was demonstrated in [45, 46] this amplitude is the same as that of the oscillating part of the instantaneous reactive power (q) for an asymmetrical three-phase system; therefore in this paper just the first one is shown. These results were obtained with balanced supply voltage at no-load. It can be concluded from the figure that simulation and experimental results have the same trend with a small error between them.

Hence, it is possible to assert that all obtained simulation results in this paper match those obtained experimentally, in this way validating the model.

5 Conclusions

A new IM dynamic model in *abc* machine variables able to represent asymmetrical SCF was proposed in this work. This model is an extension of the model proposed to represent core losses uniformly distributed in an IM core. SCF were modelled as the decrement of the equivalent core loss resistance at each phase that allows distributing the effect of the fault among the three phases.

Based on the proposed dynamic model in *abc* machine variables, two new models were deduced. The first one, in *qd0* variables, was used to implement dynamic simulations and the other, in sequence components, was used to facilitate the SCF analysis in steady state and to derive an equivalent circuit. This circuit was used to analyse the effect of SCF on the variables of the IM in steady state at rated frequency.

From this equivalent circuit and from simulation results, it was concluded that there is a good correlation between SCF severity and the magnitude of the IM stator negative sequence current. Because the IM stator negative sequence current can be easily measured, it can be used to evaluate the SCF. A drawback of this proposal appears when the IM is supplied with an unbalanced voltage that produces a similar effect, in this way it masks the SCF effect on the negative sequence current.

Aiming to avoid the effect of the unbalanced supply voltage the correlation between the SCF severity and the magnitude of the IM input negative sequence impedance as well as its real and imaginary components were also evaluated. It was concluded that there is a good correlation between the SCF severity and the negative sequence impedance magnitude and its components; therefore these variables represent other possibilities to evaluate the IM core conditions. Finally, the good correlation between the SCF severity and the amplitude increase of the $2\omega_e$ component of the active power was demonstrated.

With the objective of validating the proposed model some experimental results were presented and compared with simulation results. All the simulation results matched those obtained experimentally, which validates the theoretical proposal.

Authors would like to propose some future work. It is well known that SCF, winding turn faults and high-resistance electrical connection produce similar effects. Therefore it would be important to develop strategies to discriminate the effect of each one. Finally, it can be remarked that the models proposed in this paper can be used as tools for developing new on-line methods for SCF diagnosis.

6 Acknowledgment

This work was supported by Universidad Nacional de Río Cuarto (UNRC), Universidad Nacional del Sur (UNS), FONCyT-ANPCyT and CONICET.

7 References

[1] TALLAM R.M., LEE S.B., STONE G., *ET AL.*: 'A survey of methods for detection of stator-related faults in induction machines', *IEEE Trans. Ind. Appl.*, 2007, **43**, (4), pp. 920–933

[2] YUNG C., BONNETT A.H.: 'Repair or replace? A decision model for industrial electric motors', *IEEE Ind. Appl. Mag.*, 2004, **10**, (5), pp. 48–58

[3] YUNG C.: 'Fit to the core: advantages of a novel method for stator core repair', *IEEE Ind. Appl. Mag.*, 2008, **14**, (6), pp. 54–61

[4] TAVNER P.J., ANDERSON A.F.: 'Core fault in large generators', *IEE Proc., Electr. Power Appl.*, 2005, **152**, (6), pp. 1427–1439

[5] TOLIYAT H.A., KLIMAN G.B.: 'Handbook of electric motors' (Dekker M. Inc., New York, USA, 2004)

[6] KLIMAN G.B., LEE S.B., SHAH M.R., LUSTED R.M., NAIR N.K.: 'A new method for synchronous generator core quality evaluation', *IEEE Trans. Energy Convers.*, 2004, **19**, (3), pp. 576–582

[7] KLIMAN G.B., SHAH M.R.: 'Method and system for detecting core faults'. US Patent, December 2002

[8] BOURGEOIS J.M., LALONDE F.: 'Apparatus and method for evaluation a condition of a magnetic circuit of an electric machine'. US Patent, November 1999

[9] KLIMAN G.B., SHAH M.R., LEE S.B.: 'Differential sensor apparatus and method for laminated core fault detection'. US Patent, March 2005

[10] SUTTON J.: 'Method and apparatus for testing laminated cores of electrical machines'. US Patent, June 2003

[11] IEEE Std. 432-1992: 'IEEE guide for insulation maintenance for rotating electric machinery (5 hp to less than 10 000 hp)', 1992

[12] RIDLEY G.: 'EL CID test evaluation, 1984-96', *Power Eng. J.*, 1997, **11**, pp. 21–26

[13] POSEDEL Z.: 'Inspection of stator core in large machines with a low yoke induction method-measurement and analysis of interlamination short-circuits', *IEEE Trans. Energy Convers.*, 2001, **16**, (1), pp. 81–86

[14] LEE S.B., KLIMAN G.B., SHAH M.R., *ET AL.*: 'Experimental study of inter–laminar core fault detection techniques based on low flux core excitation', *IEEE Trans. Energy Convers.*, 2006, **21**, (1), pp. 85–94

[15] LEE S.B., KLIMAN G.B., SHAH M.R., NAIR N.K., LUSTED R.M.: 'An iron core probe based inter–laminar core fault detection techniques for generator stator cores', *IEEE Trans. Energy Convers.*, 2005, **20**, (2), pp. 344–351

[16] ORDAZ-MORENO A., ROMERO-TRONCOSO R.J., VITE-FRIAS J.A., RIVERA-GILLEN J.R., GARCIA-PEREZ A.: 'Automatic online diagnosis algorithm for broken-bar detection on induction motors based on discrete wavelet transform for FPGA implementation', *IEEE Trans. Ind. Electron.*, 2008, **55**, (5), pp. 2193–2202

[17] CUSIDÓ J., ROMERAL L., ORTEGA J.A., ROSERO J.A., ESPINOSA A.G.: 'Fault detection in induction machines using power spectral density in wavelet decomposition', *IEEE Trans. Ind. Electron.*, 2008, **55**, (2), pp. 633–643

[18] DA SILVA A.M., POVINELLI R.J., DEMERDASH N.A.O.: 'Induction machine broken bar and stator short-circuit fault diagnostics based on three-phase stator current envelopes', *IEEE Trans. Ind. Electron.*, 2008, **55**, (3), pp. 1310–1318

[19] SU H., CHONG K.T.: 'Induction machine condition monitoring using neural network modeling', *IEEE Trans. Ind. Electron.*, 2007, **54**, (1), pp. 241–249

[20] AYHAN B., TRUSSELL H.J., CHOW M.-Y., SONG M.-H.: 'On the use of a lower sampling rate for broken rotor bar detection with DTFT and AR-based spectrum methods', *IEEE Trans. Ind. Electron.*, 2008, **55**, (3), pp. 1421–1434

[21] BOSSIO G.R., DE ANGELO C.H., BOSSIO J.M., PEZZANI C.M., GARCÍA G.O.: 'Separating broken rotor bars and load oscillations on IM fault diagnosis through the instantaneous active and reactive currents', *IEEE Trans. Ind. Electron.*, 2009, **56**, pp. 4571–4580

[22] DRIF M., CARDOSO A.J.M.: 'Airgap-eccentricity fault diagnosis, in three-phase induction motors, by the complex apparent power signature analysis', *IEEE Trans. Ind. Electron.*, 2008, **55**, (3), pp. 1404–1410

[23] BLÖDT M., BONACCI D., REGNIER J., CHABERT M., FAUCHER J.: 'On-line monitoring of mechanical faults in variable-speed induction motor drives using the Wigner distribution', *IEEE Trans. Ind. Electron.*, 2008, **55**, (2), pp. 522–533

[24] GARCÍA G.O., SANTISTEBAN J., BRIGNONE S.: 'Iron losses influence on a field-oriented controller'. 20th Int. Conf. on Industrial Electronics, Control and Instrumentation, IECON 94, Bologna, Italy, September 1994, pp. 633–638

[25] LEVI E., SOKOLA M., BOGLIETTI A., PASTORELLI M.: 'Iron loss in rotor-flux-oriented induction machines: identification, assessment of detuning, and compensation', *IEEE Trans. Power Electron.*, 1996, **11**, (5), pp. 698–709

[26] DE LA BARRERA P.M., BOSSIO G.R., SOLSONA J.A., GARCÍA G.O.: 'On-line iron loss resistance identification by a state observer for rotor-flux-oriented control of induction motor', *Energy Convers. Manag.*, 2008, **49**, (10), pp. 2742–2747

[27] DE LA BARRERA P.M., BOSSIO G.R., SOLSONA J.A., GARCÍA G.O.: 'Stator core fault diagnosis for induction motors based on parameters adaptation'. Seventh IEEE Int. Symp. on Diagnostics for Electric Machines, Power Electronics and Drives (SDEMPED 2009), Cargèse, France, August–September 2009

[28] SATO T., SAKAKI Y.: 'Physical meaning of equivalent loss resistance of magnetic cores', *IEEE Trans. Magn.*, 1990, **26**, (5), pp. 2894–2897

doi: 10.1049/iet-epa.2009.0281

[29] GARCÍA G.O., MENDES LUÍS J.C., STEPHAN R.M., WATANABE E.H.: 'An efficient controller for an adjustable speed induction motor drive', *IEEE Trans. Ind. Electron.*, 1994, **41**, (5), pp. 533–539

[30] LEVI E.: 'Impact of iron loss on behavior of vector controlled induction machines', *IEEE Trans. Ind. Appl.*, 1995, **31**, (6), pp. 1287–1296

[31] ARKAN M., PEROVIĆ D.K., UNSWORTH P.: 'Online stator fault diagnosis in induction motors', *IEE Proc.-Electr. Power Appl.*, 2001, **148**, (6), pp. 537–547

[32] ENOKIZONO M., SHIMOJI H., HORIBE T.: 'Effect of stator construction of three-phase induction motors on core loss', *IEEE Trans. Magn.*, 2003, **39**, (3), pp. 1484–1487

[33] MCKINNON D., SEYOUM D., GRANTHAM C.: 'Investigation of parameter characteristics for induction machine analysis and control'. Second Int. Conf. on Power Electronics, Machines and Drives, (PEMD 2004), 31 March–2 April, 2004, vol. 1, pp. 320–325

[34] MOSES A., RAHMATIZADEH H.: 'Effects of stress on iron loss and flux distribution of an induction motor stator core', *IEEE Trans. Magn.*, 1989, **25**, (5), pp. 4003–4005

[35] DE LA BARRERA P.M., CURTI M.R., BOSSIO G.R., SOLSONA J.A., GARCÍA G.O.: 'Experimental generation and quantification of stator core faults on induction motors'. The Seventh IEEE Int. Symp. on Diagnostics for Electric Machines, Power Electronics and Drives (SDEMPED 2009), Cargèse, France, August–September 2009

[36] LEE K., HONG J., LEE K.-W., LEE S.B., WIEDENBRUG E.: 'A stator-core quality-assessment technique for inverter-fed induction machines', *IEEE Trans. Ind. Appl.*, 2010, **46**, (1), pp. 213 –221

[37] KRAUSE P.C., WASYNCZUK O., SUDHOFF S.D.: 'Analysis of electric machinery' (IEEE Press, New York, USA, 1994)

[38] PAAP G.C.: 'Symmetrical components in the time domain and their application to power network calculations', *IEEE Trans. Power Syst.*, 2000, **15**, (2), pp. 522–528

[39] YUN J., LEE K., LEE K., LEE S.B., YOO J.: 'Detection and classification of stator turn faults and high resistance electrical connections for induction machines', *IEEE Trans. Ind. Appl.*, 2009, **45**, (2), pp. 666–675

[40] YUN J., CHO J., LEE S.B., YOO J.: 'Online detection of high–resistance connections in the incoming electrical circuit for induction machines', *IEEE Trans. Ind. Appl.*, 2009, **45**, (2), pp. 694–702

[41] LEE S.B., TALLAM R.M., HABETLER T.G.: 'A robust, on-line turn-fault detection technique for induction machines based on monitoring the sequence component impedance matrix', *IEEE Trans. Power Electron.*, 2003, **18**, (3), pp. 865–872

[42] IEEE Std. 112-1996: 'IEEE Standard test procedure for polyphase induction motors and generators', 1996

[43] SOTTILE J., KOHLER J.L.: 'An on-line method to detect incipient failure of turn insulation in random-wound motors', *IEEE Trans. Energy Convers.*, 1993, **8**, (4), pp. 762–768

[44] BOSSIO G.R., DE ANGELO C.H., DONOLO P.D., CASTELLINO A.M., GARCÍA G.O.: 'Effects of voltage unbalance on IM power, torque and vibrations'. Seventh IEEE Int. Symp. on Diagnostics for Electric Machines, Power Electronics and Drives (SDEMPED 2009), Cargèse, France, August–September 2009

[45] WATANABE E., STEPHAN R., AREDES M.: 'New concepts of instantaneous active and reactive powers in electrical systems with generic loads', *IEEE Trans. Power Delivery*, 1993, **8**, (2), pp. 697–703

[46] AKAGI H., WATANABE E., AREDES M.: 'Instantaneous power theory and applications to power conditioning' (IEEE Press, 2007)

8 Appendix

8.1 Experimental generation and quantification of SCF

The method presented in [35] to generate and quantify SCF consists in introducing a copper piece into a stator slot, as shown in Fig. 10, to produce a short circuit in the core laminations. This method allows generating non-destructive faults and the experiment repeatability to study the phenomenon in depth.

The 'loop test' [11], was used to validate the proposed method. This test consists in generating the rated frequency flux inside the stator core through a test coil.

When the test coil is energised and in the presence of a fault, hot spots appear in the core that can be detected by a thermal imaging camera, as shown in Fig. 11.

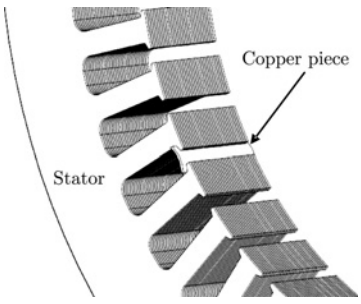

Figure 10 *Short circuit of the stator core lamination through a copper piece*

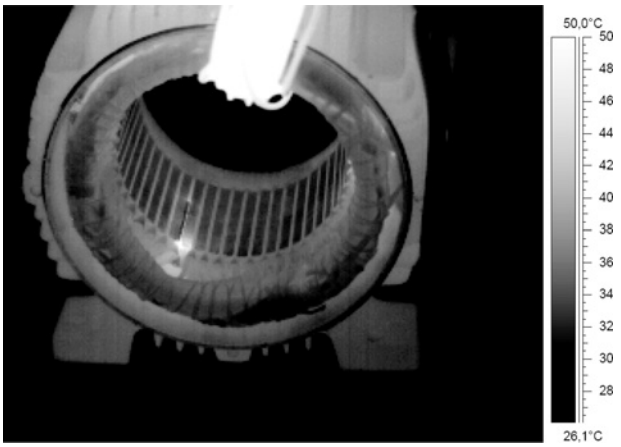

Figure 11 *Thermal image of the stator core during the loop test*

In this particular case, the severity factor is $\eta = 8.050$ (see Table 2).

In this experiment, the core temperature was measured in two different points: the area around the fault (point 1) and that between the fault and the test coil (point 2), as shown in Fig. 12.

Figs. 13*a* and *b* show temperature increase (ΔT_{core}) with respect to room temperature against time, at points 1 and 2, respectively.

From the analysis of these figures, it can be concluded that as the severity factor increases, temperature also increases in both, around the fault and in the rest of the core. It can also be observed that for more intense faults, this temperature increase is of about 15°C. That is why these faults are considered incipient for this IM. All these considerations validate the method proposed and developed in the present work.

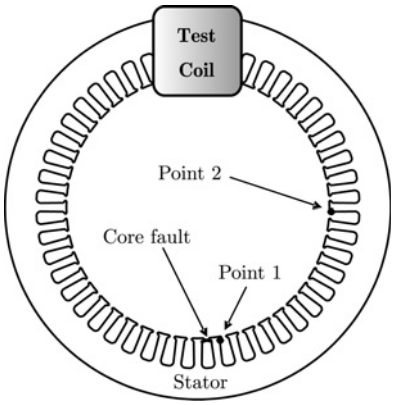

Figure 12 *Physical disposition of the test coil and the measuring points*

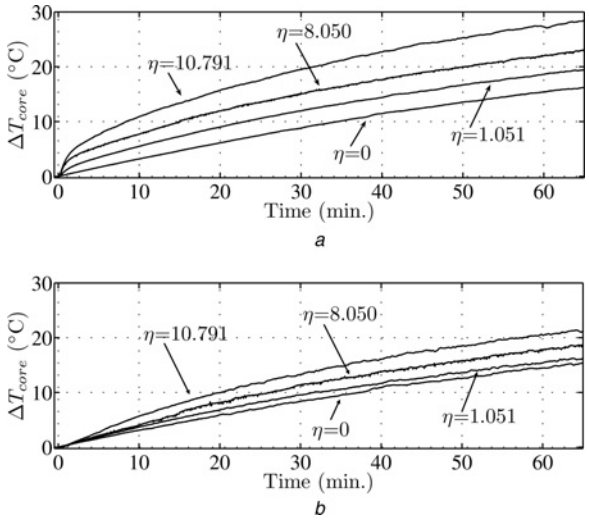

Figure 13 *Temperature increase with respect to room temperature*

a Point 1
b Point 2

doi: 10.1049/iet-epa.2009.0281